Buckling And Stoichiometry Of Zirconium Nitride Coatings On Pyrolytic Graphite Substrates

Sebastian Ritter, Jennifer L. Gray, Jeff Shallenberger, Winfrey Leigh

Ken and Mary Alice Lindquist Department of Nuclear Engineering

The Pennsylvania State University, University Park, PA 16802

Abstract—**Diversion of TRISO fuel particles from peaceful uses represents a proliferation risk. The coating of nuclear pyrolytic graphite pebbles with a thin layer of the refractory ceramic Zirconium Nitride (ZrN) may enhance spent TRISO fuel particle containment verification. To evaluate the suitability of ZrN coatings on graphite substrates, ZrN thin films are analyzed for morphological and stoichiometric properties. ZrN thin films are deposited on Highly Oriented Pyrolytic Graphite (HOPG) to simulate well oriented pyrolytic graphite in graphite pebbles. ZrN is deposited using radio frequency reactive sputtering deposition at a substrate temperature of 25 °C with a nitrogen partial pressure of 10 mTor and a 124 V DC substrate bias voltage. The resulting thin film morphology is analyzed using optical profilometry, atomic force microscopy in tapping mode, x-ray photoelectron spectroscopy, and field emission transmission electron microscopy. Film thicknesses of 85 nm to 460 nm are achieved. ZrN coating surface and bulk stoichiometry is determined to be Zr rich with a Zr to N ratio of roughly 2 to 1. A ZrO_2 layer is found at the thin film surface, which is attributed to oxygen surface diffusion. ZrN coating buckling, and cracking is observed with increasing deposition time. An exponential growth in the size of buckles as a function of deposition time is observed. It is found that buckling is attributable to delamination within the graphite substrate rather than a delamination of the ZrN coating from the substrate.**

Keywords— ZrN; TRISO; Thin Films; Protective Layer

I. Introduction

Zirconium Nitride (ZrN) is a refractory ceramic material with an electrical resistivity of tens of μΩ·cm at room temperature [1] [2]. It is widely used in industry as a hardening coating with good wear and corrosion resistance [2]. In the high-temperature pebble bed reactor design, nuclear pyrolytic graphite pebbles contain thousands of millimeter sized tri-structural isotropic (TRISO) fuel particles enclosed within the graphite matrix of a fuel pebble. The adoption of such reactor types in states under nuclear safeguards agreements poses a challenge to safeguards. One diversion path of nuclear material from peaceful purposes constitutes the removal of low burn-up TRISO fuel particles from the nuclear graphite matrix of a fuel pebble.

By coating nuclear fuel pebbles with ZrN, IAEA inspectors may be provided with an additional layer of fuel pebble integrity verification via ZrN coating integrity verification. One embodiment of such a method may use optical light to check for coating integrity. Another method may use the electrical conductivity of the ZrN coatings to validate its integrity. Whichever method is used in future safeguard inspections, ZrN coatings on nuclear pyrolytic graphite is first required to be shown a feasible endeavor.

II. Rationale

ZrN coatings are desired to show a good adhesion to pyrolytic graphite, a high density, along with a lack of cracking or buckling phenomena. The behavior of a ZrN coating may be highly dependent on the properties of the pyrolytic graphite substrate itself. In this paper, phenomena are described which are found by coating Highly Oriented Pyrolytic Graphite (HOPG) with 85 nm to 460 nm thick ZrN films via radio frequency reactive sputtering physical vapor deposition. This deposition method has been chosen for its wide adoption in the industry. HOPG is used as a substrate to simulate areas on the surface of pyrolytic graphite pebbles in which graphite crystallites may exhibit a high degree of orientation. Such high degrees of orientation are feasible to occur during the application of radial mechanical pressure during the manufacturing process of fuel pebbles. Deposited HOPG substrates are of a square cross section with a size of 1 cm by 1 cm, and 5 mm deep.

III. methodes and Deposition parameters

ZrN coatings are deposited by radio frequency reactive magnetron sputtering from a Zirconium metal target in a N_2/Ar plasma using a Kurt J Lesker CMS-18. Both feed gases N_2 and Ar are 99.99 % pure, according to its manufacturer. The base pressure of the process is $4.8 \cdot 10^{-8}$ mbar. The metallic Zirconium target is sputtered at 294 W, a power density of 41.60 W per square inch. The N_2 partial pressure is set at 10 mTorr and the Ar partial pressure is set at 48.6 mTorr. Deposition times are set at 2000 s, 5000 s, and 10000 s in three separate deposition runs yielding three separate HOPG coated samples, each of which is separately characterized. The substrate is held at 124 V DC relative to ground and is sputtered at 10 W to enhance coating density. The substrate temperature is held at 25 °C.

IV. Characterization of Zirconium Nitride Coatings

Following deposition, thin film morphology, porosity, adhesion, and stoichiometry is analyzed. Optical profilometry via the Zygo NexView 3D, Atomic Force Microscopy (AFM) in tapping mode via the Bruker Icon I, X-ray Photoelectron Spectroscopy (XPS) via the PHI Versaprobe II model PHI5000, and field emission Transmission Electron Microscopy (TEM) via the FEI Titan 3 is utilized.

A. Morphology and Porosity

Cross sectional TEM HAADF images reveal achieved film thicknesses of 85 nm to 460 nm. Qualitatively, the coating consists of columnar grains, which grow from the substrate-film interface region, forming a porous structure. Porosity arises from intergranular voids. This structure is consistent with the Zone 1 in the Thornton structure zone model [3]. Columnar grains are forming a fine morphology with humps and valleys along the surface of the coating. Via a cross-sectional TEM HAADF image, Figure 1 shows how the increase in deposition time leads to an increase in porosity and in surface roughness.
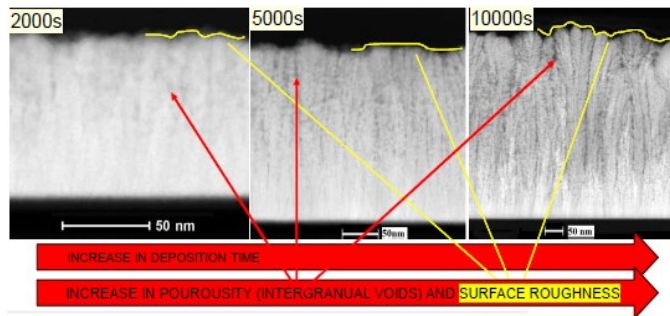

Fig. 1. Cross-sectional TEM HAADF images of the ZrN coating. A qualitative increase in the size of intergranular voids with increasing deposition time is shown. Also an increase in surface roughness s observed. The white scale on the buttom of each image is 50 nm. The deposition time is provided in the top left corner of each image. Film thickness increases with an increase of deposition time.

AFM is used for a quantitative determination of surface roughness by determining the cross-sectional columnar crystallite size. An AFM 2D topological map is created and a mask is placed on this map using the Gwyddion 2.54 software package. The size distribution of the cross-sectional columnar crystallites is fitted to a log-normal distribution with a χ^2 result of 44.4. The obtained numerical result is 13.01 nm +/- 11.49 nm with a one gaussian statistical significance for the HOPG sample deposited for 2000 s. This value has also been determined for the 10000 s deposited sample as 34.52 nm +/- 18.79 nm with a one gaussian statistical significance.

B. Adhesion

Both bucking and delamination of the ZrN coating is observed at all three deposition times. With increasing deposition time larger buckler are observed. AFM is used to quantify this result in Figure 2. An exponential growth behavior is found empirically.
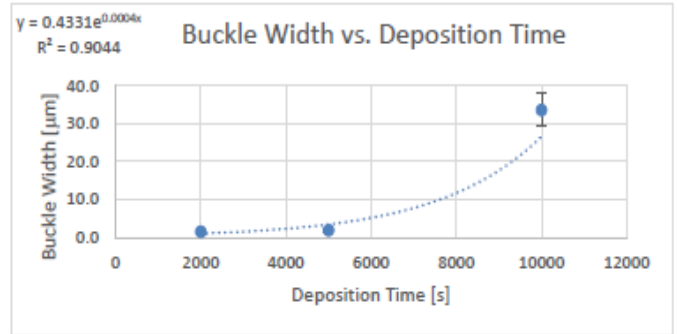

Fig. 2. The growth of the buckle width with increasing ZrN coating deposition time. Three buckle widths are randomly selected for each data point. AFM data is used. The growth empirically fits an exponential growth function shown in the top left corner.

AFM further reveals a step difference in height between the bases of buckles, indicating that buckle formation may occur preferentially along surface defects. Surface defects constituting neighboring graphene layer sheets may lower the threshold energy for delamination. Figure 3 shows a cross-sectional buckle profile. Measured step heights ranged from 4.0 nm +/- 3.2 nm to 13.2 nm +/- 5.5 nm for the 2 000 s deposited HOPG sample.
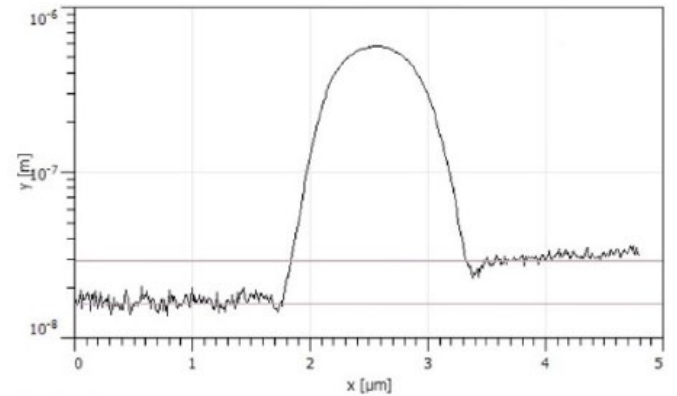

Fig. 3. An AFM cross-section profile of a buckle morphological feature found on the 2000 s ZrN deposited HOPG substrate sample. Neighboring graphene layers with a step height difference may seed the browth of buckles. This step height is measured to be 13.2 nm +/- 5.5 nm.

Optical profilometry images, such as the one presented in Figure 4, reveal smaller secondary buckles growing on extended, larger buckles. Large extended buckles are only rarely observed for shorter deposition times and dominate at long deposition times. It can be hypothesized that is phenomena arises from a delamination of graphene sheets under the tensile stress of a growing ZrN layer. It can be further hypothesized that smaller buckles only arise from a delamination of the ZrN layer from the underlying graphene sheet.
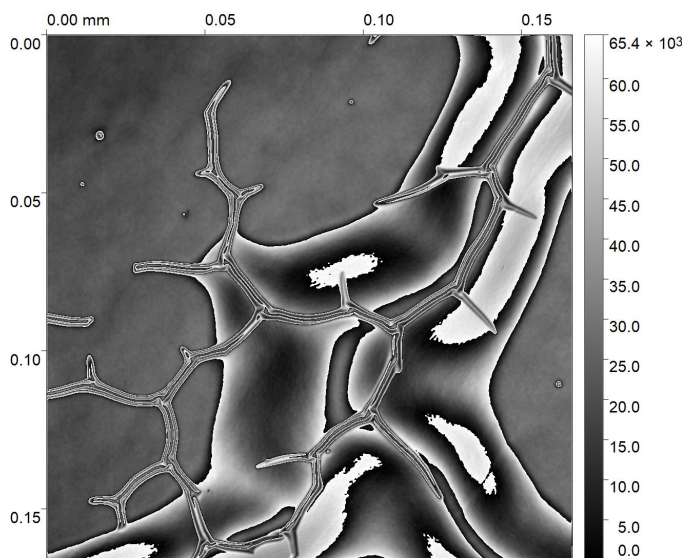
Fig. 4. An optical profilometry image of a ZrN coating deposited on a HOPG substrate for 10 000 s. The scale of the image is given in units of mm. The scale of intensity is in arbitraty units. Smaller secondary buckles are seen growing on extended buckles.

TEM with Energy-Dispersive X-ray Spectroscopy (EDS) is used to partially test these hypotheses. If they were true, one would expect a direct observation of delamination of graphene sheets from other graphene sheets with the ZrN coating firmly attached to the upper set of graphene sheets. Figure 5 shows an EDS image of a large extended buckle, with this exact phenomenon present. A TEM EDS evaluation of fine buckles and blisters reveals a lack of a Carbon layer near the delamination side of the coating.

The branching of the fine buckles resembles modelling results from Ren Hongtao et al. [4] who use a finite element model to treat thin films as an incompressible neo-Hookean solid adhering to a rigid substrate.
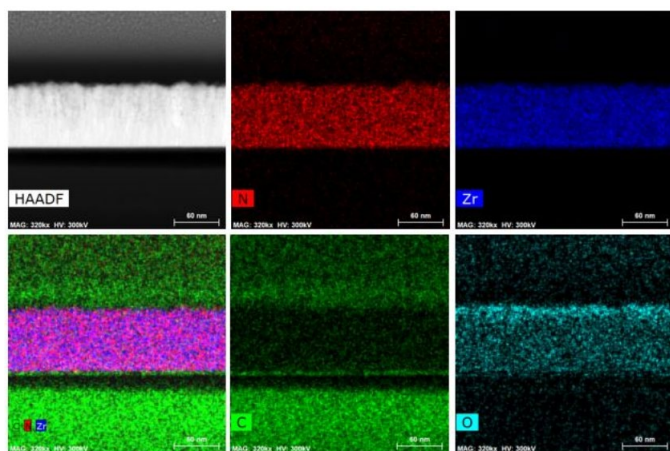

Fig. 5. A TEM EDS corss sectional image is shown of the ZrN coating deposited on a HOPG substrate for a duration of 2 000 s. The top left image shows a TEM HAADF image and each following image shows a TEM EDS image of elemental concentrations of Nitrogen, Zriconium, Carbon and Oxigen. The bottom left image shows an airgap between the ZrN coating and

the HOPG substrate with thin sheets of graphene attached to the underside of the coating. The bottom right image indicates an increase of oxigen concentration near the air exposed side of the ZrN coating.

C. Stoichometry and Oxide Formation

Figure 5 shows an increased oxygen concentration of the ZrN coating at its atmospheric exposed side. Stoichiometry of the coating is quantitively determined via XPS at the surface of the coating and 10 nm below the surface of the coating. These values are then compared with EDS measurements of the bulk of the coating. Stoichiometry is determined by comparing elemental atomic concentrations.

Figure 6 shows a plot of the resulting Zr to N ratio. For each measurement technique, there are no statistically significant variations between different coating deposition times in the measured elemental concentrations and in the measured stoichiometries. The coating is rich in Zr with a stoichiometry of roughly 2 to 1 for all deposition times. EDS bulk and XPS measurements 10 nm below the surface of the coating are in good statistical agreement. The surface stoichiometry appears poor in N with a Zr to N ratio of roughly 3. This is attributed to the oxidation of the Zr rich coating as atmospheric oxygen diffuses into the coating. At the surface, Oxygen is the dominant element with an atomic concentration of 37.1 %, dropping to 12.39 % +/- 0.49 % in the bulk material of the coating. Flour, Carbon and Silicon based surface contaminants also contribute to a high Zr/N ratio near the surface of the coating.
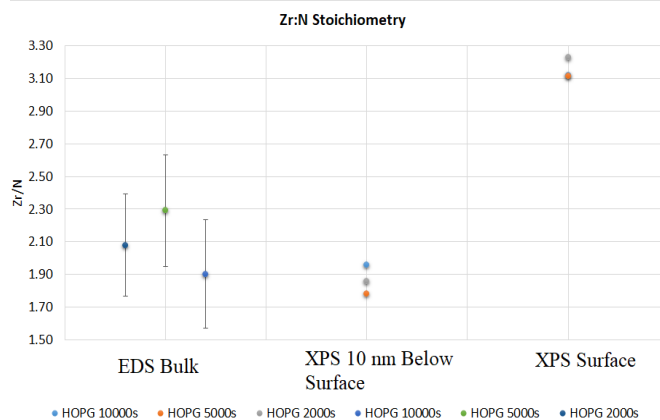

Fig. 6. The Zr to N stoichometric ratio as a function of analysis technique. XPS measurements do not indicate a one sigma error bar and represent single point measurements.

XPS measurements indicate that the surface oxygen concentration drops by roughly 50 %, when a depth of 10 nm is reached. ZrO_2 is detected as the dominant oxide compound of Zr. The occurrence of ZrO_2 within the first 10 nm of the surface is of importance in pebble bed reactors. While such a thin layer may have only marginal effects on neutronics, the formation of a ZrO_2 layer has implications on the corrosive and tribological properties of the ZrN coating. Zr oxides are known to form a protective oxide layer in the Zr cladding of nuclear fuel elements in light water reactors [5].

V. Conclusion

The electrical, mechanical, optical and corrosive properties of ZrN coatings make them an attractive coating of nuclear pyrolytic graphite pebbles for safeguard applications. However, findings of this paper indicate that growth induced stresses of ZrN coatings have negative implications on its suitability as a coating of pyrolytic graphite. It is found that the coatings of radio frequency reactive plasma vapor deposition deposited ZrN on HOPG show columnar grains, consistent with the Zone 1 in the Thornton structure zone model. It is found that the coating exhibits buckling phenomena for all analyzed film thicknesses, ranging from 85 nm to 460 nm. Fine structured buckles originating from coating delamination dominate at low film thicknesses. For films thicker than 85 nm, widely stretched buckles appear which are suggested to originate from graphene sheet delamination while the ZrN coating itself remains attached to graphene sheets. Finally, XPS and TEM EDS analyses indicate that the bulk of the ZrN coating material is rich in Zr with a roughly 2 to 1 ratio of Zr to N. The first 10 nm of the coating is found to be rich in ZrO_2, which is attributed to diffusion of atmospheric O_2 into the coating and subsequent oxidation of the Zr rich coating.

References

[1] Lengauer W. "Transition Metal Carbides, Nitrides, and Carbonitrides." Chap. 7 in *Handbook of Ceramic Hard Materials*, 202–252. John Wiley / Sons, Ltd, 2008. ISBN: 9783527618217. doi:10.1002/9783527618217.ch7.

[2] Alexander A. Gromov, Liudmila N. Chukhlomina. *Nitride ceramics: combustion synthesis, properites, and applications*. Wiley, 2014. ISBN: 9783527684533.

[3] Thornton, J. A. *Annual Review of Materials Science* 7 (1977): 239.

[4] Ren Hongtao et al. "Watching Dynamic Self-Assembly of Web Buckles in Strained MoS2 Thin Films." PMID: 30776213, *ACS Nano* 13, no. 3 (2019): 3106–3116. doi:10.1021/acsnano.8b08411.

[5] Arthur T. Motta, Donald R. Olander. *Light water reactor materials*. American Nuclear Society, 2017. ISBN: 9780894484612.